

FLOW MECHANISMS ACTIVE IN WING ROCK OF COMBAT AIRCRAFT

Lars E. Ericsson, Mountain View, California 94040, USA
and

Martin E. Beyers, Institute for Aerospace Research, Ottawa, Ontario K1A 0R6, Canada

Abstract

Whereas the wing-rock problem in general is well known, its high sensitivity to configuration details and flow conditions is not, handicapping the designer of combat aircraft that operate at high angles of attack. The present paper reviews the literature describing the flow mechanisms present in the observed wing-rock of various combat aircraft. This provides the source knowledge needed for inclusion of wing rock considerations in future combat aircraft designs and indicates the direction for future research.

Nomenclature

b	wing span
c	airfoil chord or delta wing center chord
d	maximum body diameter
f	oscillation frequency
l	Magnus lift, coefficient $c_l = l / q_\infty db$
l	rolling moment, coefficient $C_l = l / q_\infty Sb$; also length of LEX
L	lift coefficient, $C_L = L / q_\infty S$; $c_l = \partial C_l / \partial \xi$
p	rotation rate
q_∞	dynamic pressure, $= \rho_\infty U_\infty^2 / 2$
r	yaw rate
Re	Reynolds number, $Re = U_\infty d / \nu_\infty$
S	reference area, $\pi d^2 / 4$ or projected wing area
t	time
U_w	wall velocity
U_∞	freestream velocity
x	axial distance from apex
Y	side force, coefficient $C_Y = Y / q_\infty S$
z	vertical coordinate (Fig. 5)

α	angle of attack
β	angle of sideslip
Δ	increment or amplitude
ζ	dimensionless z-coordinate, $= z/c$
θ_A	forebody apex half-angle
Λ	leading-edge sweep angle
ξ	dimensionless x-coordinate $= x/c$
ρ	air density
σ	inclination of roll axis
ϕ	body-fixed roll angle
ω	frequency, $= 2\pi f$
$\bar{\omega}$	reduced frequency, $= \omega c / U_\infty$

Subscripts

CG	center of gravity (rotation center)
crit	critical
N	nose tip
VB	vortex breakdown
WR	wing rock
1,2,3	numbering subscript
∞	freestream conditions

Derivative Symbols

$$\dot{X} = \partial z / \partial t ; C_{lp} = \partial C_l / \partial (pd / 2U_\infty)$$

1 Introduction

Figure 1 illustrates the surprises awaiting the vehicle designer. [1] Tests of the X-29A aircraft [2] showed that at $\alpha < 35$ deg the wing rock was of the type occurring on straight or moderately swept wings, caused by dynamic airfoil stall. [3] When this source of wing-rock was eliminated by the use of the ailerons, forebody-induced wing rock [4,5] occurred at $\alpha > 35$ deg. Tests of the F-18 HARV aircraft [6] showed that it also exhibits wing-rock characteristics that may be of

the wing-stall variety [3] at low angles of attack and become of the forebody-induced type [4,5] at higher alphas [7] (Fig. 2). The measured roll damping of the X-31 aircraft [8] (Fig. 3) indicates that wing rock will occur at $25^\circ < \alpha < 50^\circ$. The discussion that follows describes the flow mechanisms that could generate the observed types of wing rock of combat aircraft.

2 Discussion

The aircraft geometry determines the type of flow mechanisms that can have generated the observed wing rock. [1] The straight-wing geometry in Figs. 1 and 2 causes the aircraft to experience wing rock at $\alpha < 35$ deg that is driven by the undamping rolling moment generated by dynamic stall of the wing sections during the roll-induced plunging motion, [3] whereas at $\alpha > 35$ deg the wing rock is produced by loads induced on the wing by the vortices shed from the slender forebody. [4,5] The undamped roll oscillations in Fig. 3 at $\alpha > 27$ deg likely resulted from the loads induced on the wing by vortices shed from the forebody and canard surfaces.

2.1 Conventional Wing Rock

Wing rock of aircraft with straight or moderately swept wings is caused by dynamic stall of the two-dimensional wing sections. The undamping-in-plunge measured on two common airfoil sections [9] (Fig. 4) is generated by the moving wall effect [10,11] illustrated in Fig. 5. If a straight-wing aircraft is perturbed when flying close to wing stall, the airfoil sections on the down-rolling wing half will experience the separation-promoting, adverse moving-wall effect illustrated in Fig. 5, whereas on the opposite, upstroking wing half the airfoil sections are experiencing the favorable, separation-delaying moving-wall effect. These plunging-induced effects on the flow separation will dominate the dynamic lift generation and combine to generate an undamping rolling moment. In the deep-stall region the top-side flow is completely separated, generating no significant lift contribution. Thus, the attached

flow on the windward side dominates, generating the damping trend shown in Fig. 4 for a two-dimensional airfoil at $\alpha > 17$ deg, and expected at higher angles of attack for a finite aspect ratio wing. Thus, the wing rock experienced at $\alpha > 33$ deg in Fig. 1 must have been caused by a different flow phenomenon, as is also the case for the F-18 HARV aircraft in Fig. 2 for $\alpha > 35$ deg. Through their test of a generic straight-wing aircraft configuration Brandon and Nguyen [12,13] showed that at very high angles of attack, where the wing was completely stalled, the wing rock must have been driven by loads induced on the wing by the vortices seen in their flow visualization test to be shed from the slender forebody.

2.2 Forebody-Induced Wing Rock

In subscale tests [12,13] a generic aircraft model with a pointed, axisymmetric body and a trapezoidal wing experienced wing rock oscillations that started at $\alpha = 25$ deg and reached 25 deg amplitude at $\alpha \approx 40$ deg (Fig. 6). The flow visualization [12] showed vortex-asymmetry switching similar to that observed in the test of the 80 deg delta wing. [14] It is shown in Refs. 4 and 5 that the wing rock did not result from any type of mutual interaction between the wing and the body vortices. The wing only provides the downstream surfaces on which the asymmetric vortices, generated by the asymmetric crossflow separation on the rotating forebody, can induce normal forces to produce the rolling moment that drives the roll oscillations. The vortex-switching flow mechanism is generated solely by the change of the asymmetric forebody crossflow separation and associated vortex shedding, generated by a sideslipping or rolling motion of the slender forebody.

Flow mechanisms that can cause the crossflow separation asymmetry to switch on a slender forebody are described in Ref. 15. So called geometric microasymmetries on a pointed, slender nose are able to cause the separation asymmetry and associated vortices to vary with the body roll angle. Although at these

high angles of attack freestream turbulence [16] and support vibration [17] can generate unsteady side-force behavior, it is found [18] that even the low angular rates associated with regular combat aircraft maneuvers generate moving-wall effects that can dominate over nose-microasymmetries and flow unsteadiness. Figure 7 shows experimental Magnus lift results [19] for initially laminar flow conditions (at $U_w/U_\infty = 0$). At $Re \leq 12.8 \times 10^4$ and $U_w/U_\infty \leq 0.3$ the Magnus lift is generated mainly by the separation-delaying moving wall effect on the top side, shifting the flow separation from the subcritical towards the supercritical position. On the bottom side the separation is already of the subcritical type and the adverse moving wall effect has little leverage for its separation-promoting action. For the turbulent flow conditions existing at $Re > 10^6$ a significantly larger Magnus lift is generated by the same flow process, thereby providing a certain degree of similarity between laminar and turbulent moving wall effects. This led to the following conclusion in Ref. 20. "For aircraft with clean, axisymmetric forebodies, with and without LEXs, conventional rotary tests performed at laminar flow conditions can provide the qualitative full-scale free-flight characteristics."

So called Magnus lift reversal occurs beyond a critical value of U_w/U_∞ , which varies with the Reynolds number. At low Reynolds numbers this occurs at a relatively large U_w/U_∞ , e.g. $U_w/U_\infty \approx 0.3$ for $Re = 0.128 \times 10^6$ (Fig. 7). This reversal is caused by the moving wall effect on boundary layer transition. [18] When $p > p_{crit}$ the adverse moving wall effect on the bottom side causes boundary layer transition to occur before separation, changing it from the subcritical towards the supercritical separation type. This effect completely overpowers the regular moving wall effects on the laminar flow separation and causes a more or less discontinuous loss of lift (Fig. 7). When increasing the Reynolds number to $0.26 \leq Re \times 10^{-6} \leq 0.325$ (Fig. 8) the critical value of U_w/U_∞ approaches zero. [19] In the critical Reynolds number region the flow separation is dominated

by the presence of the laminar separation bubble [18] (Fig. 9). The boundary-layer turbulence generated by the adverse moving wall effect causes early transition in the lifted shear layer forming the separation bubble, thereby delaying separation and resulting in increased suction. This process generates most of the measured negative Magnus lift in Fig. 8. The promotion of separation through the delayed transition on the opposite side also contributes to the negative Magnus lift, but to a lesser degree. The excellent flow visualization results obtained by Keener [21] (Fig. 10) show the finite extent on a pointed, ogival nose of the transitional flow separation with its laminar separation bubble. This finite separation extent is consistent with the finite Reynolds number range for which the critical flow region with its laminar separation bubble can be sustained [19] (Fig. 8).

As the Reynolds number based on body diameter was 0.26×10^6 in the test performed by Brandon et al, [12,13] the crossflow over the nose and nose shoulder occurred in the near-critical (Fig. 7) and critical (Fig. 8) flow regions. Figure 6 shows the wing rock to have started at $\alpha \approx 25$ deg. As the apex half-angle for the three caliber tangent-ogive nose is $\theta_A \approx 19$ deg, the forebody flow separation and associated vortices will in the static case be symmetric for $\alpha < 38$ deg. [15] Thus, the vortex asymmetry producing the observed wing rock is generated by the roll-rate-induced moving wall effect on the flow separation at the existing near-critical and critical flow conditions. It is shown in Ref. 22 how this type of moving wall effects on transition also can cause the oscillatory type of coning motion exhibited by a circular, flat-faced cylinder. [23] Thus, one can envision the following scenario [4,5,24] for the observed wing rock [12] (Fig. 11). For the unperturbed flow conditions at $t = t_0$, the forebody flow separation and associated vortices are symmetric until a lateral disturbance, generated by flow unsteadiness [16] or sting oscillation [17], in the tunnel test [12] initiated the rolling motion illustrated at $t = t_1$, which generated the adverse moving wall effect that caused boundary layer transition to occur, changing the crossflow

separation on that side from the subcritical to the supercritical type.

When the rolling motion is initiated at $t = t_1$, the vortex geometry at the wing is still symmetrical. However, the adverse moving wall effect on the forebody crossflow causes boundary layer transition to occur earlier in the shear layer of the laminar separation bubble, in the manner discussed earlier for the generation of negative Magnus lift (Figs. 7-9), thereby delaying the flow separation and associated vortex formation on that side. Due to time-lag effects, similar to those for slender wing rock, [25] this vortex geometry is not realized at the wing until $t = t_1 + \Delta t$, when the vortex-induced loads on the wing act to initiate a reversal of the rolling direction. (For clarity, only the dominating vortex closest to the body is shown for $t > t_1$). When the roll rate reaches its maximum in the opposite direction at $\phi = 0$, another reversal of the forebody separation-asymmetry and associated vortex shedding is initiated. Because of the time lag effect, [4] the vortex geometry at the (now horizontal) wing is the same as at $t = t_1 + \Delta t$, in agreement with the flow visualization results. [12] During the time lag Δt the vortex-induced, statically stabilizing rolling moment acts to reverse the rolling motion, generating through the associated time lag effects [26] an undamping rolling moment that drives the observed wing rock.

It should be noted that the amplitude-increase generates increased moving wall effects from half-cycle to half-cycle, increasing the separation-asymmetry and associated vortex-asymmetry, which in turn generates an increase of the vortex-induced loads and the associated rolling moment that drives the oscillation. Thus, during the amplitude build-up the vortex-induced rolling moment is increasing rapidly with every half-cycle until reaching the maximum flow-separation and associated vortex asymmetry. This accounts for the rapid half-cycle-to-half-cycle growth of the oscillation amplitude [12] (Fig. 12) compared to that for the 80 deg delta wing [14] (Fig. 13).

This type of rapid amplitude growth can only occur at $\alpha < 2\theta_A$. At $\alpha > 2\theta_A$ the separation

asymmetry with associated vortex-induced rolling moment is constant, independently of what the roll rate is. [15] This is demonstrated by Fidler's results for a pointed ogive-cylinder [27] (Fig. 14). At $\alpha = 55 \text{ deg} > 2\theta_A = 45 \text{ deg}$, the roll rate p_N of the nose tip only determines the direction of the generated side force C_Y , but has no effect on its magnitude. Whereas in the Langley test [12] (Fig. 6) the bearing friction supplied part of the needed damping, in free flight the wing alone must supply all the damping needed at very high angles of attack to limit the growth of the wing rock amplitude. [28,29] The experimental results [30] in Fig. 15 show that for NACA-0012 and -0015 airfoil shapes the plunging-induced roll damping will be substantial in the alpha range $20 \text{ deg} < \alpha < 50 \text{ deg}$, in dramatic contrast to the undamping being generated at $10 \text{ deg} < \alpha < 20 \text{ deg}$ in two-dimensional flow [9] (Fig. 4), which contributed to the wing-rock generated by the finite-aspect-ratio wing of the X-29A and F/A-18 aircraft at $\alpha < 35 \text{ deg}$ (Figs. 1 and 2).

2.2.1 F/A-18 Wing Rock

The current F/A-18 combat aircraft exhibits a variation of the described forebody-induced wing rock at $\alpha > 35 \text{ deg}$ (Fig. 2). Interaction between vortices generated by the forebody and LEX surfaces, [7] shown in Fig. 16 for steady flight conditions at $\alpha = 38.7 \text{ deg}$ and $\beta = \phi = 0$ (Ref. 31) are prevalent at $30 \text{ deg} \leq \alpha \leq 50 \text{ deg}$. [32] The figure illustrates how the forebody vortex at a high angle of attack interacts with the LEX vortex on that side of the body. To understand the character of the LEX vortex that is experiencing breakdown, it is constructive to consult the experimental results for a 60-deg delta-wing-body model [33] (Fig. 17). The figure shows that although the suction peaks are reduced significantly downstream of a spiral vortex breakdown they are still of significant magnitude. The "dead-air" type of flow region does not materialize until the vortex breakdown reaches the delta-wing apex. Consequently, the interaction between the forebody and LEX vortices took the form shown in Fig. 18 between a tightly wound forebody vortex and a loosely

wound LEX vortex that is undergoing spiral vortex breakdown. The LEX vortex, even in the spiraling form (judging by Fig. 17), would possess a significant portion of its regular capability to increase the wing lift. The experimental amplitude time history, recorded in the water tunnel test [6] (Fig. 19), indicates that the unperturbed vortex geometry, shown for $t = t_0$ in Fig. 18, lasted a significant time before a lateral disturbance was generated by tunnel flow unsteadiness [16] and/or sting oscillation [17] that was of large enough magnitude to initiate the rolling motion indicated at $t = t_1$.

The moving wall effect, generated on the forebody by the rolling motion, delays flow separation on one side and promotes it on the opposite side, generating the vortex geometry shown for $t = t_1$ in Fig. 18. When the forebody vortices reach the wing at $t = t_1 + \Delta t$, only the vortex closest to the body interacts with the spiraling LEX vortex, lifting it away from the LEX surface and thereby diminishing its capacity to increase the wing lift on that side of the body. The time-lag effect, which causes this statically stabilizing vortex interaction to generate undamping, [7,34] is well illustrated by flight-test results [35] (Fig. 20). The maximum roll rate, generated at $\phi = 0$, produces the delay of forebody crossflow separation that causes the lowering of the forebody vortex, enabling it to interact with the spiraling LEX vortex at $|\phi| \approx 20$ deg, decreasing the wing lift on that side. The result is that a statically stabilizing rolling moment is created that through the associated time lag effect [26] generates the undamping that drives the wing rock, similarly to what was the case for the generic configuration discussed earlier (Fig. 11). The interaction of the forebody vortex with the LEX-induced lift generation on the wing is less forceful than the direct interaction with the wing occurring in the case of the generic configuration, [12] resulting in a slower amplitude build-up [6] (Fig. 19) than in that case [12] (Fig. 12).

The wing-rock amplitude, observed in full-scale flight of the F/A-18 HARV aircraft, and also measured in wind tunnel tests at low Reynolds numbers, [6] shows the amplitude to

increase with angle of attack, from 3 deg at $\alpha = 30$ deg to 21 deg at $\alpha = 45$ deg (Fig. 2). When the angle of attack is increased further, however, the limit-cycle amplitude abruptly starts to decrease rapidly, becoming zero when α approaches 55 deg. Events that could cause this to happen are: (1) The breakdown of the LEX vortex is approaching the LEX apex, effectively eliminating any spiraling, vortex-like flow structure that the forebody vortex can interact with to influence the wing lift, (2) The angle of attack has reached the limit of the range $\alpha < 2\theta_A$ within which roll-rate-induced moving wall effects can control the asymmetric crossflow separation and associated asymmetric body vortices. [36,37] Additionally, when the vortex breakdown reaches the LEX apex, the wing enters its deep-stall region where the windward-side attached flow dominates, generating damping that increases rapidly with increasing angle of attack into the deep-stall region. (See earlier discussion of Fig. 15). Further investigation [32] has shown that extensive unsteady vortex interactions also occur at $45 \text{ deg} \leq \alpha \leq 55 \text{ deg}$, which tend to eliminate the flow conditions capable of generating wing rock.

One difficulty with the experimental data base for the F-18 combat aircraft (Fig. 2) is to fully understand the reason for the good agreement between subscale test data and full-scale flight results. Accounting for the damping provided by the bearing friction in the subscale test [6] would at most double the difference between the wind tunnel data and the flight test results. [7] The agreement would still remain remarkably good. Considering the dominant role played by the viscous moving wall effects this was initially a great surprise. Further study [32] has revealed how the combination of differing flow conditions could have caused this agreement to occur between full-scale-flight and wind-tunnel-test results at widely different Reynolds numbers. One powerful reason is that the breakdown location of the LEX vortex is relatively insensitive to a three orders of magnitude change of the Reynolds number [38,39] (Fig. 21). Another reason is that the effective outer portion of the LEX geometry is

found to be relatively unaffected by viscous fairing effects on the effective fuselage geometry, probably because the dominating rollrate-induced effects on the LEX camber controlled the vortex asymmetry.

In order to have more realistic expectations from subscale tests it is prudent to relate experiences of the opposite type. In the AGARD-FDP special course on Aircraft Dynamics at High Angles of Attack, held at NASA Langley Research Center, 8-11 April, 1991, Dr. R. C. Nelson, University of Notre Dame, showed a film clip of the observed wing rock of the F/A-18 aircraft. [40] The flow visualization results, obtained on the full-scale aircraft as well as on the subscale model in a water tunnel, both showed an extensive interaction between forebody and LEX vortices, resulting in large amplitude wing rock [6] (Fig. 2). In the repetition of the AGARD-FDP special course at the von Karman Institute in Brussels, Belgium, Nelson revealed that testing a larger F-18 model in the wind tunnel at the NASA Langley Research Center, at a much higher Reynolds number than in the Notre Dame water tunnel, [6] Nguyen et al had not observed any wing rock at all. Nelson thought that this was an illustration of the difficulties discussed in Ref. 41. He was right. [42] It is clear from the discussion of Figs. 7-9 that the moving wall effect on flow separation is reversed if instead of affecting the separating boundary layer directly it influences separation via its effect on boundary layer transition. The situation was the opposite to that encountered in an earlier test of a generic aircraft model. [12] In that case tests at NASA Langley Research Center (in the same tunnel and at the same Reynolds number) showed wing rock to exist (Figs. 6 and 12), whereas it would not occur for laminar flow conditions, and would be much less severe or non-existent at full-scale Reynolds numbers. [4,36]

3 Conclusions

Whereas on a typical combat aircraft with its modestly swept wing dynamic stall of wing sections can cause wing rock at modest angles of attack, $\alpha < 35$ deg, the main concern is the

wing rock generated at high angles of attack, $\alpha > 35$ deg, through the flow field induced on the wing by the vortices from a slender forebody. In one case critical forebody crossflow conditions can generate vortices that induce loads on the wing that drive the wing rock. In the other case laminar or turbulent forebody crossflow conditions generate vortices that interact with the spiral flow structure of the LEX vortex undergoing vortex breakdown, thereby modifying the wing loads to produce the rolling moment that drives the wing rock. It should be emphasized that considerable care is needed in planning the subscale tests of combat aircraft in such a way that they can produce flow fields sufficiently similar to those encountered in full-scale flight.

References

- [1] Ericsson, L. E., "Various Sources of Wing Rock," *J. Aircraft*, Vol. 27, No. 6, 1990, pp. 488-494.
- [2] Fratello, D. J., Croom, M. A., Nguyen, L. T., and Domack, C. S., "Use of the Updated NASA Langley Radio-Controlled Drop-Model Technique for High-Alpha Studies of the X-29A Configuration," *AIAA Paper 87-2559*, Aug. 1987.
- [3] Ericsson, L. E. and Reding, J. P., "Fluid Mechanics of Dynamic Stall, Part I, Unsteady Flow Concepts," *J. Fluids and Structures*, Vol. 2, Jan. 1988, pp. 1-33.
- [4] Ericsson, L. E., "Wing Rock Generated by Forebody Vortices," *J. Aircraft*, Vol. 26, No. 2, 1989, pp. 110-116.
- [5] Ericsson, L. E., "Further Analysis of Wing Rock Generated by Forebody Vortices," *J. Aircraft*, Vol. 26, No. 12, 1989, pp. 1098-1104.
- [6] Quest, T., Nelson, R. C., and Fisher, D. F., "A Study of High-Alpha Dynamics and Flow Visualization for a 2.5% Model of the F-18 HARV Undergoing Wing Rock," *AIAA Paper 91-3267*, Sept. 1991.
- [7] Ericsson, L. E., "Separated Flow Mechanics in F-18 Wing Rock," *J. Aircraft*, Vol. 33, No. 1, 1996, pp. 81-86.
- [8] Klein, V. and Noderer, K. D., "Aerodynamic Parameters of the X-31 Drop Model Estimated from Flight Data at High Angles of Attack," *AIAA Paper 92-4357*, Sept. 1992.
- [9] Liiva, J., Davenport, F. J., Gray, L., and Walton, I. C., "Two-Dimensional Tests of Airfoils Oscillating Near Stall," *TR 68-13*, April 1968, U S Army Aviation Labs, Fort Eustis, VA.
- [10] Ericsson, L. E. and Reding, J. P., "Unsteady Airfoil Stall, Review and Extension," *J. Aircraft*, Vol. 8, Aug. 1971, pp. 609-616.

- [11] Ericsson, L. E., "Moving Wall Effect in Relation to Other Dynamic Stall Flow Mechanisms," *J. Aircraft*, Vol. 31, No. 6, 1994, pp. 1303-1309.
- [12] Brandon, J. M. and Nguyen, L. T., "Experimental Study of Effects of Forebody Geometry on High Angle of Attack Stability," *J. Aircraft*, Vol. 25, No. 7, 1988, pp. 591-597.
- [13] Brandon, J. M., Murray, D.G., and Nguyen, L. T., "Experimental Effects of Fuselage Geometry on High Angle of Attack Static and Dynamic Stability and Control," ICAS-86-5.4.1, Sept. 1986.
- [14] Nguyen, L. E., Yip, L. P., and Chambers, J. R., "Self-Induced Wing Rock of Slender Delta Wings," AIAA Paper 81-1883, Aug. 1981.
- [15] Ericsson, L. E. and Reding, J. P., "Asymmetric Flow Separation and Vortex Shedding on Bodies of Revolution," *Tactical Missile Aerodynamics : General Topics*, edited by M. J. Hensch, Vol. 141 of *Progress in Astronautics and Aeronautics*, 1989, pp. 391-452.
- [16] Ericsson, L. E. and Reding, J. P., "Vortex Unsteadiness on Slender Bodies at High Incidence," *Journal of Spacecraft and Rockets*, Vol. 24, No. 4, 1987, pp. 319-326.
- [17] Ericsson, L. E., "Lateral Oscillations of Sting-Mounted Models at High Alpha," *Journal of Spacecraft and Rockets*, Vol. 27, No. 5, 1990, pp. 508-513.
- [18] Ericsson, L. E., "Moving Wall Effects in Unsteady Flow," *J. Aircraft*, Vol. 25, No. 11, 1988, pp. 977-990.
- [19] Swanson, W. M., "The Magnus Effect: A Summary of Investigations to Date," *Journal of Basic Engineering*, Vol. 83, Sept. 1961, pp. 461-470.
- [20] Ericsson, L. E. and Beyers, M. E., "Wind-Tunnel Aerodynamics in Rotary Tests of Combat Aircraft Models," *J. Aircraft*, Vol. 35, No. 4, 1997, pp. 521-528.
- [21] Keener, E. R., "Flow Separation Patterns on Symmetric Forebodies," NASA TM-86016, Jan. 1986.
- [22] Ericsson, L. E. and Reding, J. P., "Dynamics of Forebody Flow Separation and Associated Vortices," *J. Aircraft*, Vol. 22, No. 4, 1985, pp. 329-335.
- [23] Yoshinaga, T., Tate, A., and Inoue, K., "Coning Motion of Slender Bodies at High Angles of Attack in Low Speed Flow," AIAA Paper 81-1899, Aug. 1981.
- [24] Ericsson, L. E. and Mendenhall, M. R., "On Forebody-Induced Wing Rock," AIAA Paper 94-0167, Jan. 1994.
- [25] Ericsson, L. E., "The Fluid Mechanics of Slender Wing Rock," *J. Aircraft*, Vol. 3, No. 5, 1984, pp. 322-328.
- [26] Ericsson, L. E., "Prediction of High-Alpha Vehicle Dynamics," ICAS-90-3.5.1, Sept. 1990.
- [27] Fidler, J. E., "Active Control of Asymmetric Vortex Effects," *J. Aircraft*, Vol. 18, No. 4, 1981, pp. 267-272.
- [28] Ericsson, L. E., "Effect of Deep-Stall Wing Dynamics on Forebody-Induced Wing Rock," *J. Aircraft*, Vol. 34, No. 3, 1997, pp. 448-450.
- [29] Ericsson, L. E., Mendenhall, M. R., Perkins Jr., S. C., "Review of Forebody-Induced Wing Rock," *J. Aircraft*, Vol. 33, No. 4, 1995, pp. 253-259.
- [30] Raghunathan, S., Harrison, J. R., and Hawkins, B. D., "Thick Airfoil at Low Reynolds Numbers and High Incidence," *J. Aircraft*, Vol. 25, No. 7, 1988, pp. 669-671.
- [31] Fisher, D. F., DelFrate, J. H., and Zuniga, F. A., "Summary of In-Flight Flow Visualization Obtained from the NASA High Alpha Research Vehicle," NASA TM-101734, Jan. 1991.
- [32] Beyers, M. E. and Cai, H. J., "F/A-18 Post-Stall Aerodynamic Database," Report LTR-AL-0088, Dec. 2001.
- [33] Bergmann, B., Hummel, D., and Oelker, H-Chr., "Vortex Formation over a Close-Coupled Canard-Wing-Body Configuration in Unsymmetrical Flow," Paper 14, AGARD CP-494, July 1991.
- [34] Ericsson, L. E., "F-18 Wing Rock Considerations," ICAS 94-2.4.2, Sept. 1994.
- [35] Fisher, D. F., DelFrate, J. H., and Richwine, D. M., "In-Flight Flow Visualization Characteristics of the NASA F-18 High Alpha Research Vehicle at High Angles of Attack," NASA TM 4193, May 1990.
- [36] Ericsson, L. E., "Unsteady Separation on Slender Bodies at High Angles of Attack," *Journal of Spacecraft and Rockets*, Vol. 30, No. 6, 1993, pp. 689-695.
- [37] Ericsson, L. E. and Beyers, M. E., "Forebody Flow Control at Conditions of Naturally Occurring Separation Asymmetry," *J. Aircraft*, Vol. 39, No. 2, 2002, pp. 252-261.
- [38] Beyers, M. E. and Ericsson, L. E., "Why is LEX Vortex Breakdown on the F/A-18 Configuration Insensitive to Reynolds Number?", AIAA Paper 2001-0690, Jan. 2002.
- [39] Beyers, M. E., "From Water Tunnel to Post-Stall Flight Simulation-The F/A-18 Investigation, Invited AIAA Paper 2002-0699, Jan. 2002.
- [40] Nelson, R. C., "Unsteady Aerodynamics of Slender Wings," AGARD -R-776, April 1991. (The F-18 wing rock results were only shown in the oral presentation).
- [41] Ericsson, L. E., "Effects of Transition on Wind Tunnel Simulation of Vehicle Dynamics," *Progress of Aerospace Sciences*, Vol. 27, 1990, pp. 121-144.
- [42] Beyers, M. E. and Ericsson, L. E. "The Challenge of Determining Combat Aircraft Wing Rock Through Subscale Testing," (to be published).

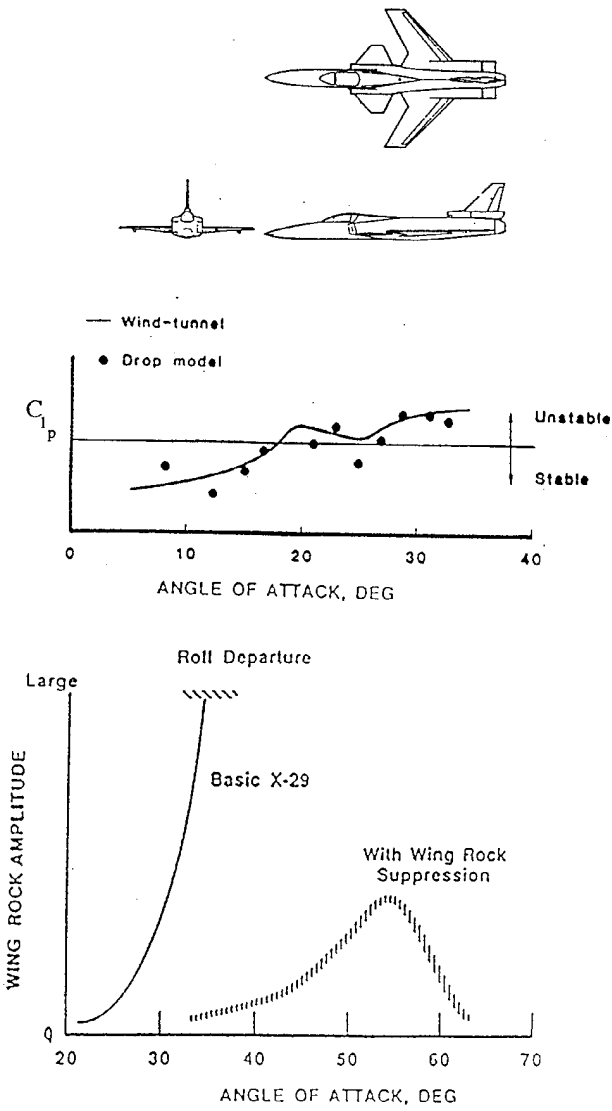


Fig. 1 Roll damping and wing rock amplitudes of the X-29A aircraft [2].

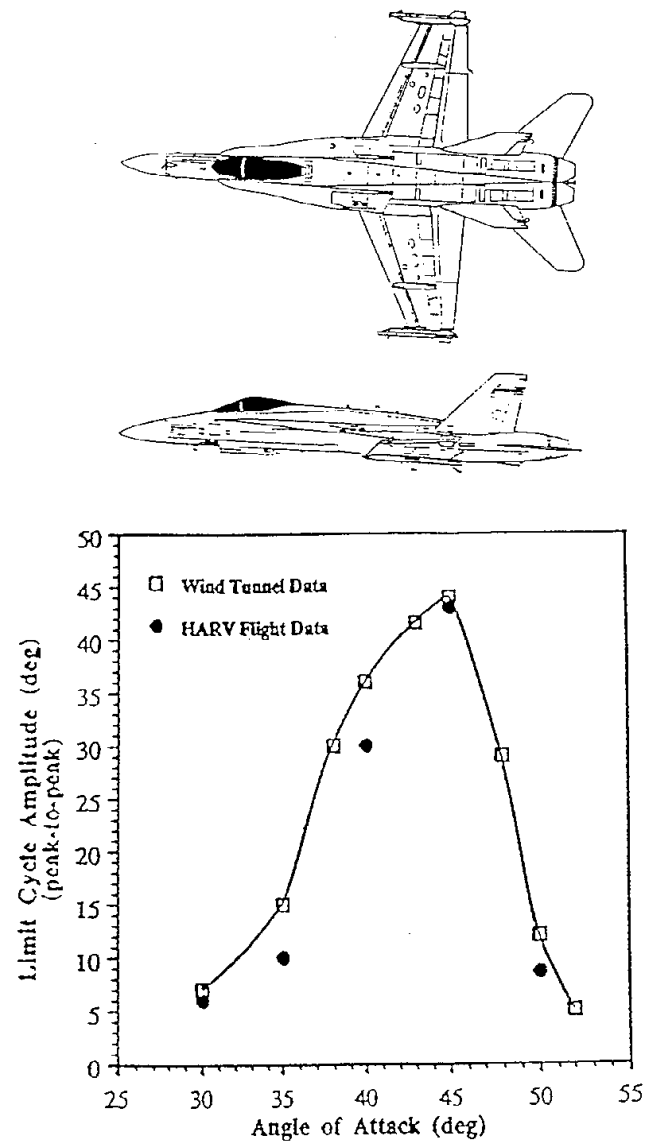
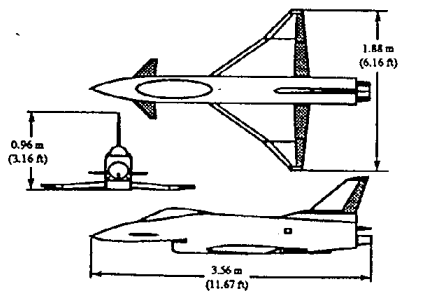


Fig. 2 Wing rock of the F-18 HARV aircraft [6].

FLOW MECHANISMS ACTIVE IN WING ROCK OF COMBAT AIRCRAFT



○ Drop model : single maneuvers
 ○ Drop model : partitioned data
 — Wind tunnel
 + Full-scale aircraft

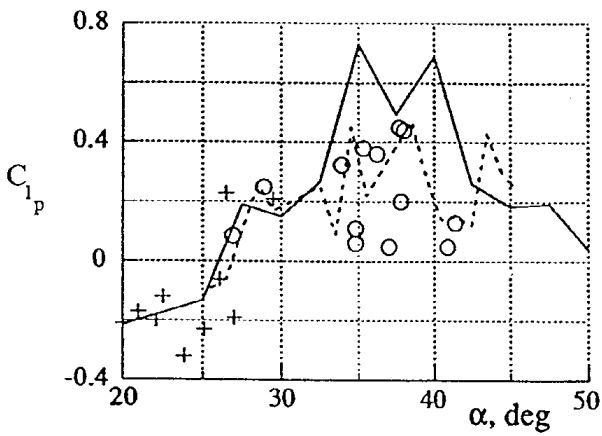


Fig. 3 Roll damping of the X-31 aircraft [8].

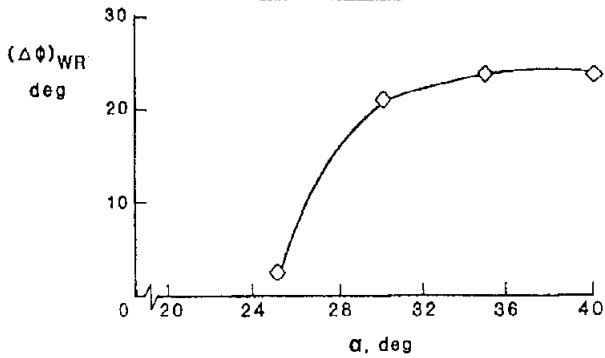
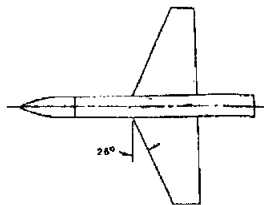


Fig. 6 Measured wing rock amplitude of wing-body configuration [12].

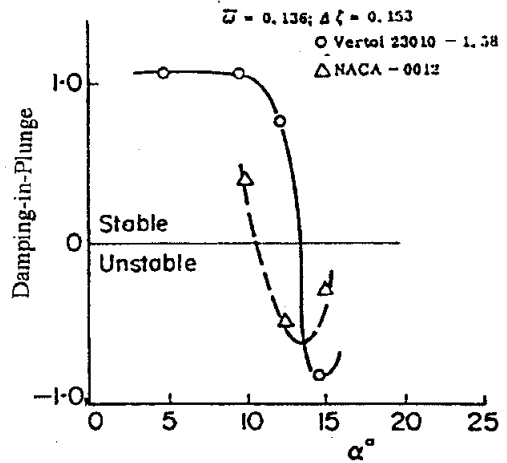


Fig. 4 Plunging-induced undamping of two common airfoil shapes [9].

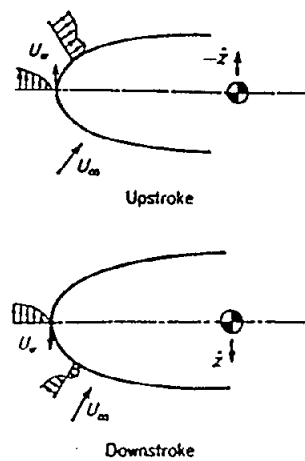


Fig. 5 Moving wall effect on a plunging airfoil [10,11].

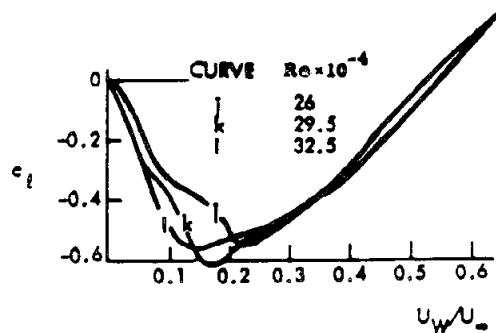


Fig. 8 Measured Magnus lift on a rotating cylinder at critical flow conditions [19].

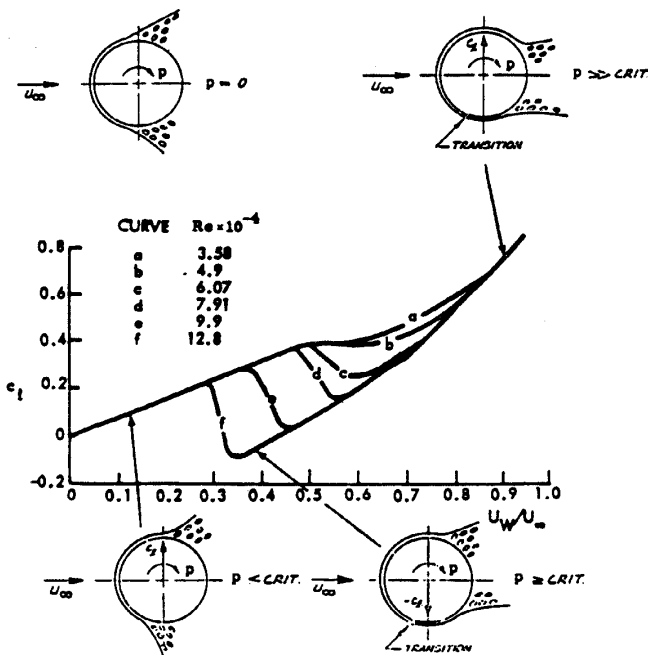
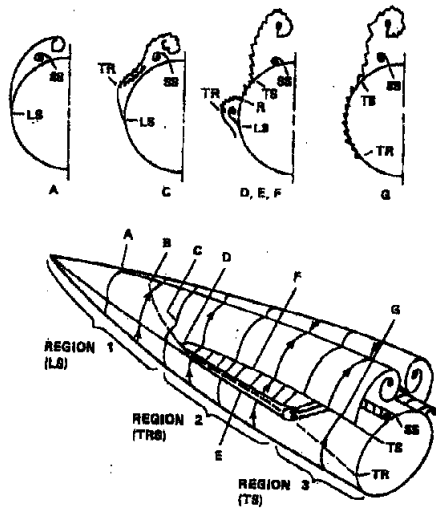


Fig.7 Moving wall effect on a rotating circular cylinder at initially ($U_w = 0$) laminar flow conditions [19].



- PRINCIPAL FEATURES:
- ① PRIMARY LAMINAR SEPARATION, LS
 - ② PRIMARY TRANSITIONAL SEPARATION, TRS = (LS + TR + TS)
 - ③ PRIMARY TURBULENT SEPARATION, TS
 - ④ SECONDARY SEPARATION, SS

Fig. 10 Oil flow visualization results for a pointed 3.5 caliber ogive at $\alpha = 55$ deg. [21].

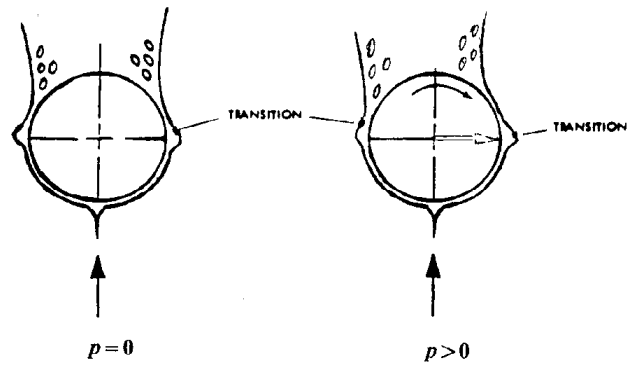


Fig. 9 Moving wall effect on the laminar separation bubbles on a circular cylinder rotating at critical flow conditions [18].

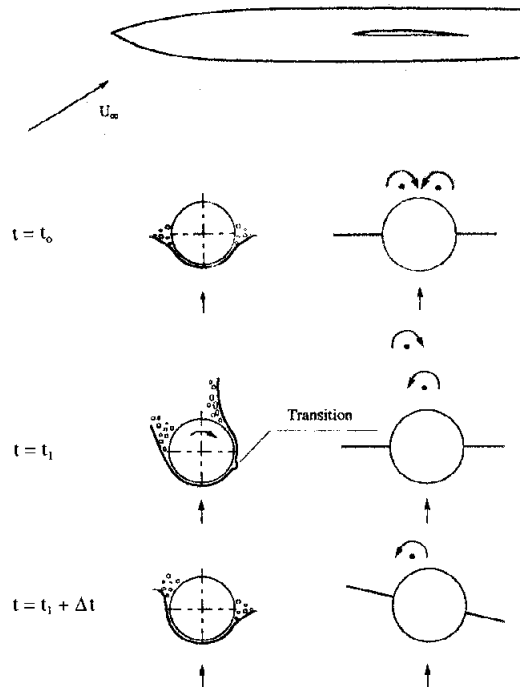


Fig. 11 Conceptual flow mechanism for forebody-induced wing rock [4,5].

FLOW MECHANISMS ACTIVE IN WING ROCK OF COMBAT AIRCRAFT

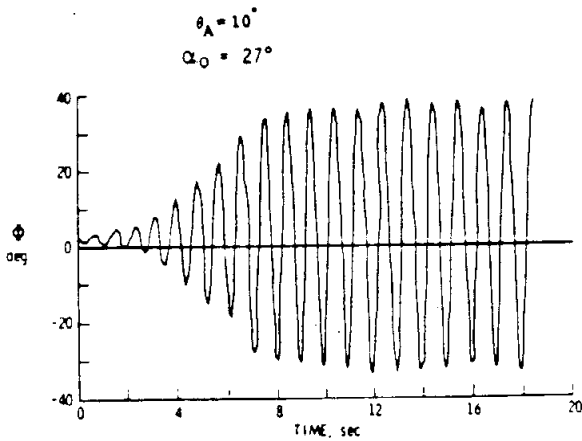


Fig. 13 Amplitude buildup during wing rock of an 80 deg delta wing [14].

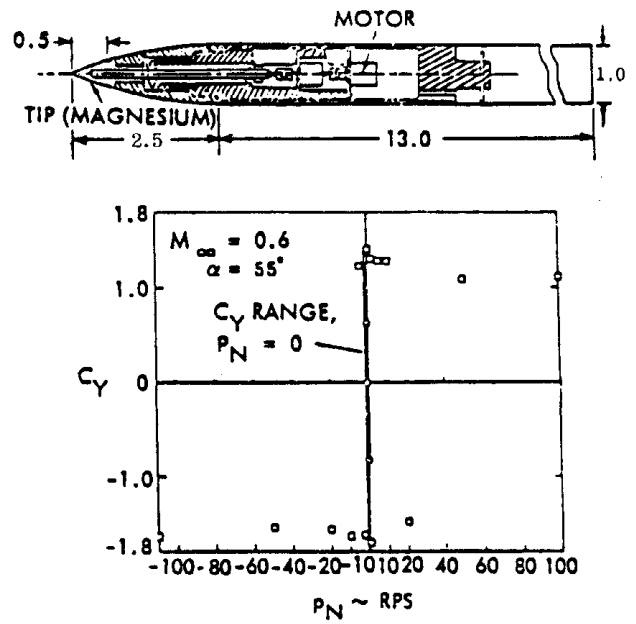


Fig. 14 Effect of spinning nose tip on vortex-induced side force at $\beta = 0$ and $\alpha = 55$ deg. [27].

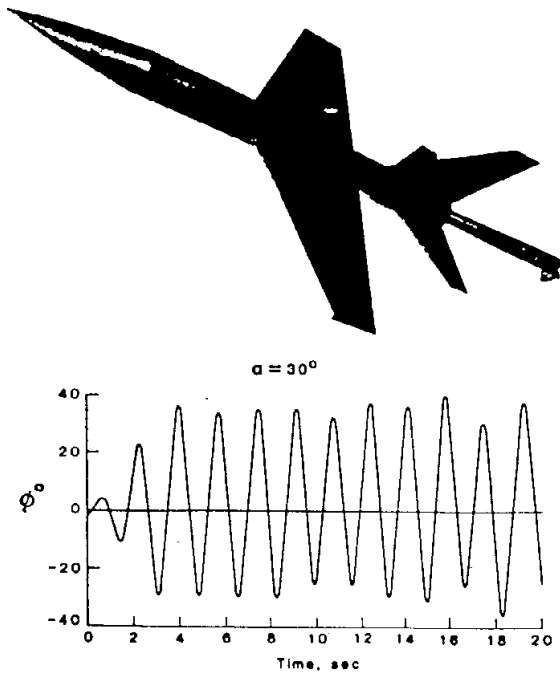


Fig. 12 Amplitude buildup during wing rock of generic aircraft configuration with a pointed forebody [12].

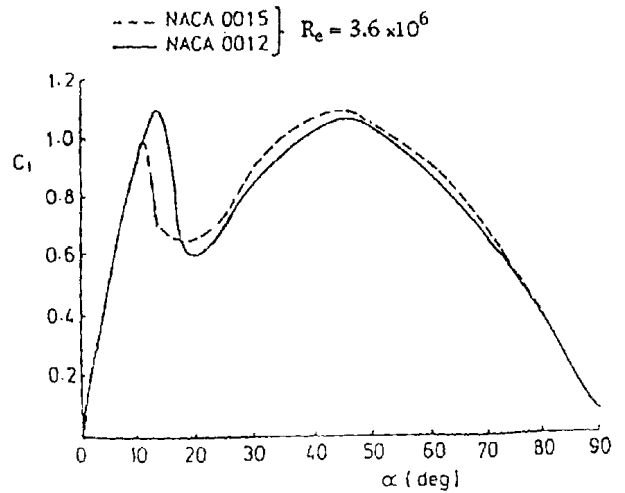


Fig. 15 Lift characteristics $c_l(\alpha)$ from 0 to 90 deg for NACA-0012 and NACA-0015 airfoils [30].

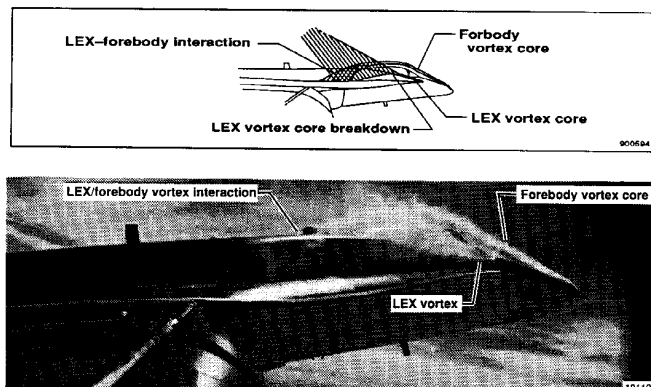


Fig. 16 Interaction between forebody and LEX vortices on the F-18 (HARV) at $\alpha = 38.7$ deg and $\beta = 0$ [31].

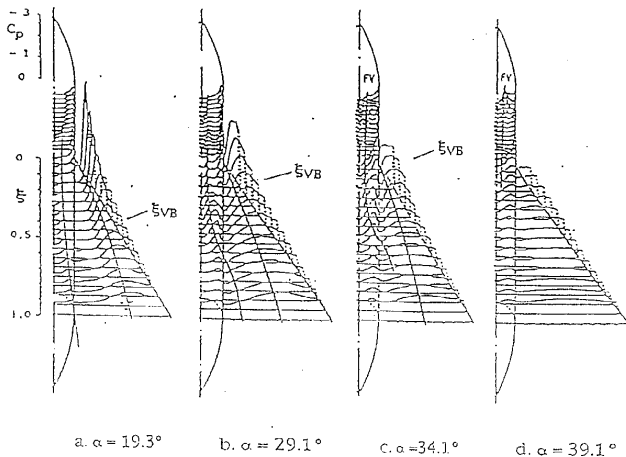


Fig. 17 Suction-side pressure distribution on 60-deg delta-wing-body model at $Re = 1.4 \times 10^6$ [33].

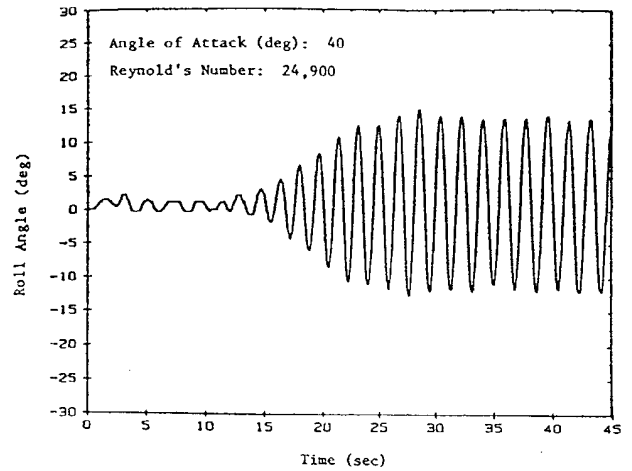


Fig. 19 Wing rock amplitude time history of subscale F-18 (HARV) model at $\alpha = 40$ deg and $Re = 0.0249 \times 10^6$ [6].

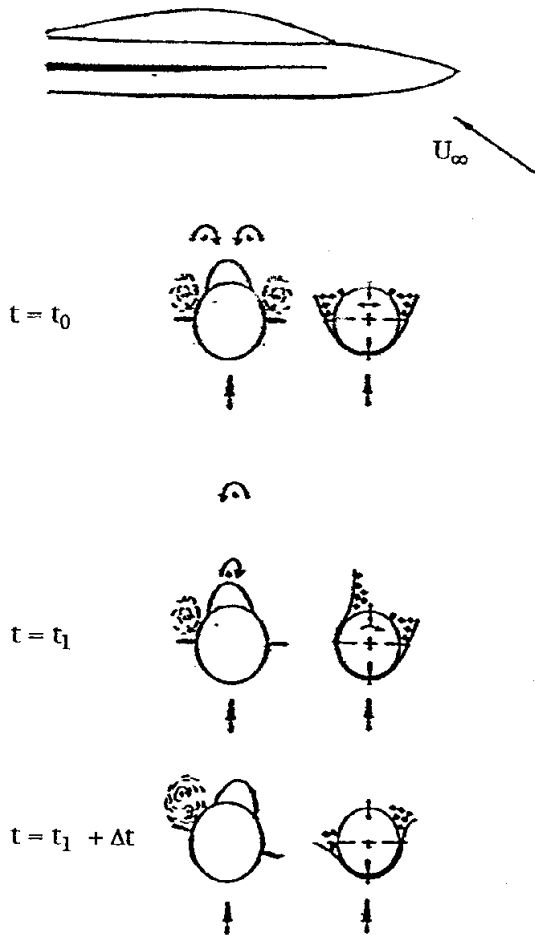


Fig. 18 Conceptual flow mechanism for LEX-forebody vortex interaction.

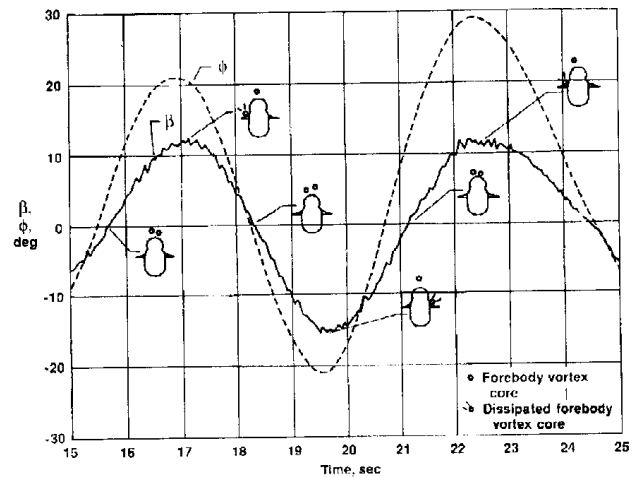


Fig. 20 In-flight roll angle time history of the F-18 (HARV) during wing rock at $\alpha \approx 45$ deg. [35].

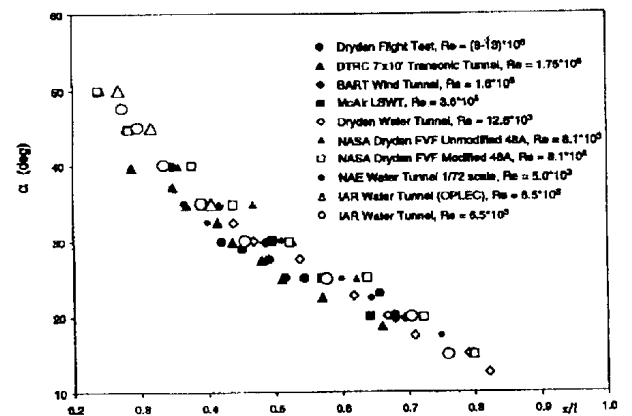


Fig. 21 Correlation of F/A-18 LEX vortex breakdown location over an extensive Reynolds number range [38,39].